A Systematic Study on Direct Photon Production from Central Heavy Ion Collisions

Fu-Ming Liu*
Institute of Particle Physics, Central China Normal University, Wuhan, China

Klaus Werner
Laboratoire SUBATECH, University of Nantes - IN2P3/CNRS - Ecole des Mines, Nantes, France
(Dated: February 2, 2008)

We investigate the production of direct photons in central Au-Au collisions at the relativistic Heavy-Ion Collider (RHIC) at 200 GeV per nucleon, considering all possible sources. We treat thermal photons emitted from a quark-gluon plasma and from a hadron gas, based on a realistic thermodynamic expansion. Hard photons from elementary nucleon-nucleon scatterings are included: primordial elementary scatterings are certainly dominant at large transverse momenta, but also secondary photons from jet fragmentation and jet-photon conversion cannot be ignored. In both cases we study the effect of energy loss, and we also consider photons emitted from bremsstrahlung gluons via fragmentation.

PACS numbers: 25.75.-q,12.38.Mh

I. INTRODUCTION

The formation and observation of a quark-gluon plasma in heavy ion collisions is an important goal of modern nuclear physics. Even if a quasiequilibrated plasma is created for a brief time in the collisions, it is still a challenge to infer knowledge of the plasma from particle production. Among those proposed "probes" of the plasma are the directly produced real photons. Those photons interact only electromagnetically, and so their mean free paths are typically much larger than the transverse size of the hot dense matter created in the collisions. As a result, high-energy photons produced in the interior of the plasma usually pass through the surrounding matter without interaction, carrying information directly from wherever they were formed to the detector.

One expects to deduce properties of the highly excited matter, in particular it's space-time evolution. Direct photons may provide these informations in two different ways: via so-called "thermal photons" emitted directly from hot and dense matter, and via secondary photons from initially produced jets. There are two kinds of such secondary photons: they may originate from the "fragmentation" of jets, or the "conversion" of jets into photons via interactions of jets with the partons of the equilibrated matter. Such secondary photons compete, however, with the photons directly produced in an initial hard nucleon-nucleon scattering, in the following referred to as "primordial NN scattering" contribution, so a carefully study of these photons is very important. In the following, we will shortly review these different photon sources.

Primordial NN scattering. The direct photon production via Compton scattering and quark-antiquark annihilation can be calculated in perturbation theory, using the usual parton distribution functions. In principle one should consider at this stage also higher order contributions, like bremsstrahlung of photons accompanying for example two-jet production in hards parton-parton scattering. However, we consider this as part of the so-called jet fragmentation (or bremsstrahlung) contribution, which will be affected by the thermalize matter, and which we will discuss separately.

Thermal photons. In high energy nuclear collisions, the density of secondary partons is so high that the quarks and gluons rescatter and eventually thermalize to form a bubble of hot quark-gluon plasma (QGP).The plasma expands and decreases its energy density so that a phase transition to hadronic gas (HG) phase appears. Thermal photons can be produced during the whole history of the evolution, from the QGP phase, the mixed phase, and from the pure HG phase. Photons from a thermal source are exponentially damped so that the contribution to very high p_{T} is negligible. However, its contribution to low p_{T} is dominant.

Jet-photon conversion. When jets pass through thermalized matter, they may interact. In case of the quark-gluon plasma, these interactions are elastic collisions between jets and deconfined partons. There is first of all quark-antiquark annihilation and quark-gluon Compton scattering, which both can produce a photon. These photons are affected by the plasma in two ways: obviously the plasma is needed to allow these interactions, but there is also a secondary effect, since the jets first of all lose energy in the plasma, before contributing to the photon production.

Jet fragmentation or bremsstrahlung photons. Photon production also occurs as higher order effect in purely partonic initial hard scatterings: at any stage of the evolution of a jet (final state parton emissions), there is a possibility of emitting photons. Also here the presence of a QGP will affect the results, since the jets lose energy during the fragmentation process. And not to forget the fragmentation contribution from induced gluon

*Electronic address: liufm@iopp.ccnu.edu.cn

radiation in the plasma.

Our paper is organized as follows: in sections 2 and 3, we discuss thermal photon production; in section 4, we study hard photons from primordial NN scattering (leading order); in section 5 we study jet-photon conversion, including the modification due to jet energy loss; in section 6 we compute photon production from jet fragmentation, also referred to as bremsstrahlung's photons, again considering the effect of energy loss; in section 7 we finally collect our results and compare with experimental data.

II. PHOTON EMISSION RATES

Thermal photon production is obtained by integrating the photon emission rate R (number of reactions per unit time per unit volume which produce a photon) over the space-time history of the expanding hot and dense matter. In this section we study the photon emission rates from different phases of the hot dense matter.

The spectral photon emissivity directly reflects the dynamics of real photon production reactions in thermalized matter. Commonly employed formalisms are finite-temperature field theory and kinetic theory. As systematically studied by Kapusta *et al.*[1], the thermal emission rate of photons with energy E and momentum $\vec{p}$ from a small system (compared to the photon mean free path) is

$$E\frac{dR}{d^3p} = \frac{-2}{(2\pi)^3}\mathrm{Im}\Pi^{R,\mu}_{\mu}\frac{1}{\exp(E/T)-1} \qquad (1)$$

where $\Pi^{R,\mu}_{\mu}$ is the retarded photon self-energy at finite temperature T. This formula has been derived both perturbatively and nonperturbatively. It is valid to all orders in the strong interaction. If the photon self-energy is approximated by carrying out a loop expansion to some finite order, then the formulation of Eq. (1) is equivalent to relativistic kinetic theory, where the emission rate of photons with energy E and momentum $\vec{p}$ from a process of type 1+2→3+γ reads

$$E\frac{dR}{d^3p} = \int(\prod_{i=1}^{3}\frac{d^3p_i}{(2\pi)^3 2E_i})(2\pi)^4\delta^{(4)}(p_1^\mu+p_2^\mu-p_3^\mu-p_\gamma^\mu) \times|\mathcal{M}|^2\,\frac{f_1(E_1)f_2(E_2)[1\pm f_3(E_3)]}{2(2\pi)^3} \qquad (2)$$

where the f's are the Fermi-Dirac or Bose-Einstein distribution functions as appropriate. Eq.(2) is convenient if the scattering amplitude, M, is evaluated in a perturbative expansion. Non-perturbative (model) calculations at low and intermediate energies, on the other hand, are more amenable to the correlator formulation, Eq.(1). In the hadronic medium, *e.g.*, Π_{em} can be directly related to vector-meson spectral functions within the vector dominance model (VDM). Instructive investigation on photon emission rates from both QGP and HG phases can be found in [1][11].

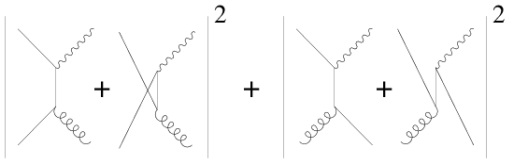

Figure 1: Two-to-two particle processes contributing to the leading order photon emission rate.

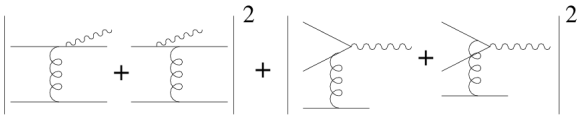

Figure 2: Bremsstrahlung and pair production contributing to photon emission. The bottom line in each diagram can represent either a quark or a gluon.

A. Quark-Gluon Plasma

In [1], the thermal rate from a quark gluon plasma is computed using the kinetic theory formalism for the simplest two-to-two scattering diagrams such as the QCD Compton process $qg\to\gamma q$ and annihilation $q\bar{q}\to g\gamma$, see Fig.1. In case of a large photon energy, and with the energy of two initial partons being larger than the energy of the output photon ($E_1+E_2>E\gg T$), the approximation $f_1(E_1)f_2(E_2)\to\exp[-(E_1+E_2)/T]$ is employed. Because the light quark masses are set to zero, an infrared cutoff $-k_c^2$ must be placed on the four-momentum transfer. The infrared divergence is regulated by an infinite resummation of finite-temperature Feynman diagrams, following Braaten and Pisarski. This amounts to a careful treatment of a small part of phase space left out in the kinetic theory calculation by imposing the infrared cutoff. When the contributions from the two regions of phase space – below and above the cutoff – are added, the result is independent of the cutoff. This provides a parameterized thermal emission rate of photons with energy E and momentum $\vec{p}$ from an equilibrated QGP at temperature T and zero net baryon density, for large values of $x=E/T$, given as

$$E\frac{dR^{\mathrm{QGP}\to\gamma}}{d^3p} = \sum_{i=1}^{N_f}(\frac{e_i}{e})^2\frac{\alpha\alpha_S}{2\pi^2}T^2\mathrm{e}^{-x}\ln\left(1+\frac{2.912}{4\pi\alpha_s}x\right) \qquad (3)$$

An additive "1" has been introduced in the argument of the logarithm to enable extrapolation to small x [1].

As noticed in Ref.[2] , Eq.(3) does not yet comprise the full result to leading order in the strong coupling constant α_s. Due to collinear singularities, bremsstrahlung as well as pair annihilation graphs contribute at the same order as the resumed 2→2 processes, c.f. Fig.2. The full result, which also necessitates the incorporation of Landau-Pomeranchuk-Migdal (LPM) interference effects,

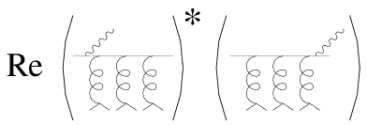

Figure 3: An interference term, involving amplitudes for photon emission before and after multiple scattering events, which contributes to the leading order emission rate.

as shown in Fig.3, has been computed in Ref.[3] as

$$E\frac{dR^{\rm QGP\to\gamma}}{d^3p} = \sum_{i=1}^{N_f}(\frac{e_i}{e})^2\frac{\alpha\alpha_S}{2\pi^2}T^2\frac{1}{e^x+1} \times\big[\ln(\frac{\sqrt{3}}{g})+\frac{1}{2}\ln(2x)+C_{22}(x) +C_{\rm brems}(x)+C_{\rm ann}(x)\big] \quad (4)$$

with convenient parameterizations of the 3 functions C as [3]

$$C_{22}(x)=\frac{0.041}{x}-0.3615+1.01{\rm e}^{-1.35x} \quad (5)$$

$$C_{\rm brems}(x)+C_{\rm ann}(x) = 0.633x^{-1.5}\ln(12.28+1/x)+\frac{0.154x}{(1+x/16.27)^{0.5}}\ . \quad (6)$$

We will employ the above formula, taking $N_f=3$, and a temperature dependent running coupling constant[4]

$$\alpha_s(T)=\frac{6\pi}{(33-2N_f)\ln(8T/T_c)}. \quad (7)$$

Effects from non-zero baryon density and from off-equilibrium are not included, the above rates can be considered to be a good approximation for the midrapidity region of Au+Au collisions at 200 AGeV. In Fig.7 we show photon emission rate from QGP. The dashed line represents the results obtained by Kapusta *et al*[1], summarized in eq.(3), the solid line refers to the calculations of AMY[3], given in eq.(4), with additional contributions compared to [1]. We can see the full contribution to photon emission from a QGP is much higher than the one from $2\to 2$ partonic processes.

B. Hadronic Matter

Photons can also be produced in a hadronic phase, from several elementary interactions, see Fig.4. The dominant contribution comes from the reactions $\pi\pi\to\rho\gamma$ and $\pi\rho\to\pi\gamma$; The decay $\rho\to\pi+\pi+\gamma$ also contributes significantly. Interactions involving strange mesons or baryons can also produce photons, but these contributions are relatively small because of the phase space suppression due to their big masses. The situation of thermal photon radiation rates from a hadronic gas is uncertain, due to difficulties related to the strong coupling

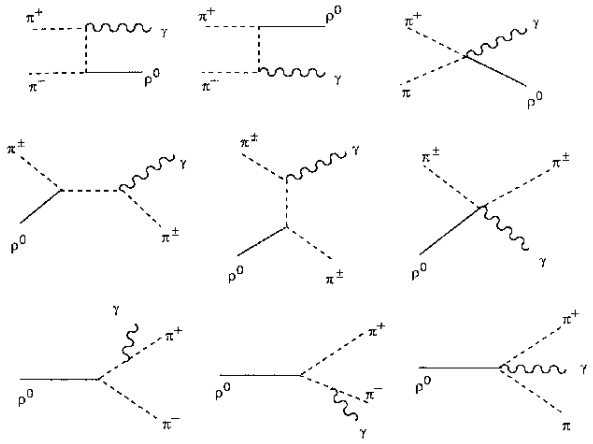

Figure 4: Photon production reactions and decays involving charged pions (dashed lines) and neutral ρ mesons (solid lines).

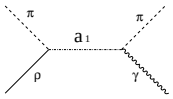

Figure 5: Feynman diagram of $\pi\rho\to\pi\gamma$ through $a_1(1260)$ resonance.

and the masses of hadrons. The study is usually carried out within effective Lagrangians. Constraints on the interaction vertices can, to a certain extent, be imposed by symmetry principles (*e.g.*, e.m. gauge and chiral invariance). Coupling constants are estimated by adjusting to measured decay branchings in the vacuum. Thus, for the temperature ranges relevant to practical applications, T=100-200 MeV, the predicted emission rates are inevitably beset with significant uncertainties, and therefore a careful judgment of the latter becomes mandatory.

Investigations along these lines were initiated in Ref.[1], where the photon self-energy has been computed to 2-loop order for a mesonic system consisting of sharp (zero width) π-, η- and ρ-mesons (plus direct $\omega\to\pi^0\gamma$ decays). In Ref.[5] it was pointed out that $\pi\rho\to\pi\gamma$ scattering via $a_1(1260)$ resonance formation (or, equivalently, $a_1\to\pi\gamma$ decay), c.f. Fig.5, constitutes an important contribution. This was followed up by a systematic treatment[6] of an interacting $\pi\rho a_1$ system to 2-loop order within the Massive Yang-Mills (MYM) framework of introducing axial-/vector mesons into a chiral Lagrangian, and, later, within the Hidden-Local Symmetry (HLS) approach[7]. The effect on in-medium vector and axial-vector meson masses is studied by Song and Fai [8].

We will use the results of the MYM calculation [9], where photon production from strangeness bearing mesons has been included as well as the axial meson a_1 as exchange particle for non-strange initial states. We show these rates in fig.6, and we list the corresponding param-

eterized rates, in unit of $\mathrm{fm}^{-4}\mathrm{GeV}^{-2}$, with the photon energy (E) and the temperature (T) both in GeV:

$$E\frac{dR_{\pi+\rho\to\pi+\gamma}}{d^3p} = T^{2.8}exp\Big(\frac{-(1.461T^{2.3094}+0.727)}{(2TE)^{0.86}} + (0.566T^{1.4094}-0.9957)\frac{E}{T}\Big) \quad (8)$$

$$E\frac{dR_{\pi+\pi\to\rho+\gamma}}{d^3p} = \frac{1}{T^5}exp\Big(-(9.314T^{-0.584} - 5.328)(2TE)^{0.088} + (0.3189T^{0.721}-0.8998)\frac{E}{T} \quad (9)$$

$$E\frac{dR_{\rho\to\pi+\pi+\gamma}}{d^3p} = \frac{1}{T^2}exp\Big(-\frac{(-35.459T^{1.126}+18.827)}{(2TE)^{(-1.44T^{0.142}+0.9996)}} - 1.21\frac{E}{T}\Big) \quad (10)$$

$$E\frac{dR_{\pi+K^*\to K+\gamma}}{d^3p} = T^{3.75}exp\Big(-\frac{0.35}{(2TE)^{1.05}} + (2.3894T^{0.03435}-3.222)\frac{E}{T}\Big) \quad (11)$$

$$E\frac{dR_{\pi+K\to K^*+\gamma}}{d^3p} = \frac{1}{T^3}exp\Big(-(5.4018T^{-0.6864} - 1.51)(2TE)^{0.07} - 0.91\frac{E}{T}\Big) \quad (12)$$

$$E\frac{dR_{\rho+K\to K+\gamma}}{d^3p} = T^{3.5}exp\Big(-\frac{(0.9386T^{1.551}+0.634)}{(2TE)^{1.01}} + (0.568T^{0.5397}-1.164)\frac{E}{T}\Big) \quad (13)$$

$$E\frac{dR_{K^*+K\to\pi+\gamma}}{d^3p} = T^{3.7}exp\Big(\frac{-(6.096T^{1.889}+1.0299)}{(2TE)^{(-1.613T^{2.162}+0.975)}} - 0.96\frac{E}{T}\Big) \quad (14)$$

Parameterisations for $K^* \to K+\pi+\gamma$ and $K+K \to \rho+\gamma$ do not appear because their rates have been found to be negligible.

Hadrons are composite objects, so they may need vertex form factors to simulate finite hadronic size effect, in particular at high momentum transfer. How much will form factor influence the results? Form factors are a very delicate subject, especially when electromagnetism and its gauge invariance are involved. For those nonstrange reaction channels as originally studied by Kapusta *et al.* [1], considering form factors provide a typical net suppression compared to the bare graphs by an appreciable factor of ~ 3 at photon energies around $E \simeq 2.5$ GeV. The reduction of the rate introduced by Rapp *et al.* [9] in $2 \sim 3$ GeV region of photon energies amount to a factor of ~ 4, confirming roughly Kapusta's findings.

In ref. [12], for each hadronic vertex appearing in the amplitudes, it is proposed to take hadronic form factor for t-channel meson X-exchange according to

$$F(\bar{t}) = \left(\frac{2\Lambda^2}{2\Lambda^2 - \bar{t}}\right)^2 \quad (15)$$

with Λ=1GeV and $\bar{t}$ being the average momentum transfer $\bar{t} = -2Em_X$, where E is the photon energy and m_X the mass of the hadron X. In our calculation, we follow this procedure: The photon emission rate is taken to be the sum of all terms in eqs. (8-14), with each term multiplied by $F^4(\bar{t})$. The corresponding curve is shown in Fig.7 as the dashed-dotted line. The dotted line is the photon emission rate without considering hadronic form factors. The form factors of Eq.(15) makes the suppression stronger compared to [1, 9]. For example, at a photon energy of $E = 2.5$ GeV, the suppression factor is about 10 for π-exchange contributions, and even 625 for K-exchange processes. The suppression are even larger for higher photon energies. So the hadronic emission rate is reduced considerably after including the hadronic form factor as in Eq.(15). The HG rate is therefore much smaller than QGP one (full line).

III. THERMAL PHOTONS FROM THE EXPANDING HOT AND DENSE MATTER

The expanding thermalized matter is treated by employing three-dimensional hydrodynamics. We compute initial conditions at some given proper time τ_0, expressed via energy density $\varepsilon(\tau_0)$, net flavor density $f_q(\tau_0)$, and collective velocity $\vec{v}(\tau_0)$, by employing the EPOS model [14, 15]. The hydrodynamic evolution is realized using SPheRIO [16], which is a "Smoothed Particle Hydrodynamics" implementation, a method originally developed in astrophysics, and later adapted to relativistic heavy ion collisions . The three-dimensional hydrodynamics describes the space-time evolution of the hot dense matter created in heavy ion collisions, via the 3-velocity $\vec{v}$, the energy density ε, the entropy density s and the baryon number density n_B, as functions of the space-time position (η, τ, r, ϕ), with η being the space-time rapidity, and r, ϕ the transverse coordinates. In this paper, we consider central AuAu collisions (10% most central events) at 200 AGeV. The corresponding results of a hydrodynamical evolutions is shown in Fig.8, where we plot the r–dependence of ε at $\eta = 0$ for different values of ϕ and τ. The initial time is $\tau_0 = 0.5\,\mathrm{fm/c}$. The solid lines and the corresponding dotted lines refer to $\phi = 0$ and $\phi = \pi/2$, respectively. The three horizontal dotted lines are the the energy densities $\varepsilon_1 = 1.675$ GeV/fm^3 and $\varepsilon_2 = 0.325$ GeV/fm^3 , limiting the mixed phase, and the freeze-out energy density $\varepsilon_3 = 0.08$ GeV/fm^3..

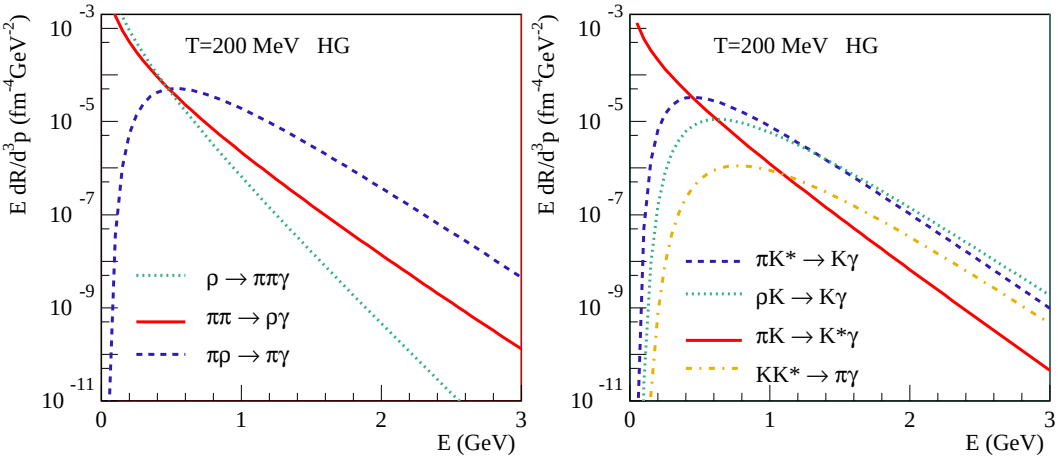

Figure 6: Photon emission rates from a HG from the different reactions (bare graphs, no hadronic form factor).

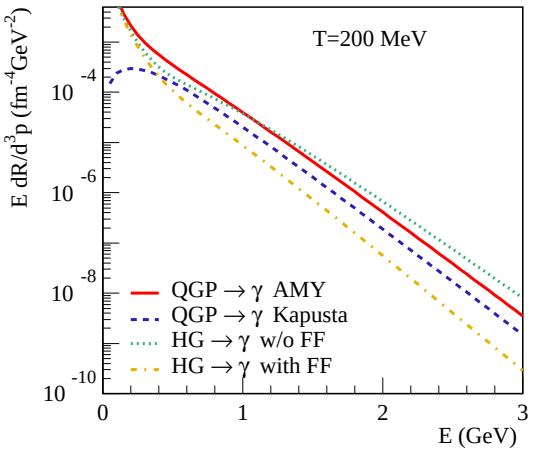

Figure 7: Photon emission rate from QGP and from HG. The dashed line represents Kapusta's *et al*[1] calculations of photon emission rates from a QGP at 200 MeV via $2 \to 2$ processes, *i.e.*, QCD Compton process and quark-antiquark annihilation. The solid line refers to AMY[3], where in addition the LPM contribution was taken into account. The dotted line is a sum of photon emission rates from a HG via different reactions (bare graphs) shown in fig. 6. The dotted dashed line stands for photon emission rates from a HG including hadronic form factors.

The relation between energy density and temperature, $T = T(\varepsilon)$, as used in SPheRIO is shown in Fig.9 (and tabulated for later use).

We define $f_{\rm QGP}$ to be the fraction of matter in the QGP phase and $f_{\rm HG}$ as the corresponding fraction in the HG phase, at each space-time point (x, y, η, τ). We have obviously $f_{\rm QGP} = 1$, $f_{\rm HG} = 0$, if the energy density is bigger than ε_1, $f_{\rm QGP} = 0$, $f_{\rm HG} = 1$, if the energy density is between ε_3 and ε_2, and $f_{\rm QGP} = 0$, $f_{\rm HG} = 0$, if the energy density is smaller than ε_3. In the mixed phase ($\varepsilon_2 < \varepsilon < \varepsilon_1$, we have $s_1 f_{\rm QGP} + s_2 f_{\rm HG} = s$, with s_1 and s_2 being the entropy densities corresponding to ε_1 and ε_2, s is the total entropy, which is simply a linear function of ε , like $s = a\epsilon + b$. Then $f_{\rm QGP}$ and $f_{\rm HG}$ are linear in ε as well, namely

$$f_{\rm QGP} = (1 - f_{\rm HG}) = \frac{\varepsilon - \varepsilon_2}{\varepsilon_1 - \varepsilon_2}. \tag{16}$$

The photon emission rates discussed in the previous chapter are obtained in the local rest frame, so we should better write

$$\Gamma(E^*, T) = E^* \frac{dR}{d^3p^*}(E^*, T) = E^* \frac{dN}{d^3p^* d^4x^*}, \tag{17}$$

where quantities viewed in the local rest frame are decorated with the superscript $*$. Bare symbols (without *) refer to the laboratory frame. We need the photon spectrum observed in the laboratory, which is given as

$$\begin{aligned} \frac{dN}{dyd^2p_{\rm T}} &= E\frac{dN}{d^3p} = \int d^4x \Gamma(E, T) \\ &= \int d^4x \Gamma(E^*, T) \\ &= \int d\tau dx dy d\eta \tau \Gamma(E^*, T), \end{aligned} \tag{18}$$

with

$$\Gamma(E^*, T) = f_{\rm QGP}\Gamma^{\rm QGP\to\gamma}(E^*, T) + f_{\rm HG}\Gamma^{\rm HG\to\gamma}(E^*, T) \tag{19}$$

where $\Gamma^{\rm QGP\to\gamma}(E^*, T)$ and $\Gamma^{\rm HG\to\gamma}(E^*, T)$ are the photon emission rates from QGP phase and from HG phase as discussed in the previous chapter. The center-of-mass energy E^* in eq.(18) is related to the photon momenta in the observer frame (appearing on the l.h.s. of Eq.(18)) as

$$E^* = \gamma E - \gamma \vec{v}(\tau, x, y, \eta) \cdot \vec{p}, \tag{20}$$

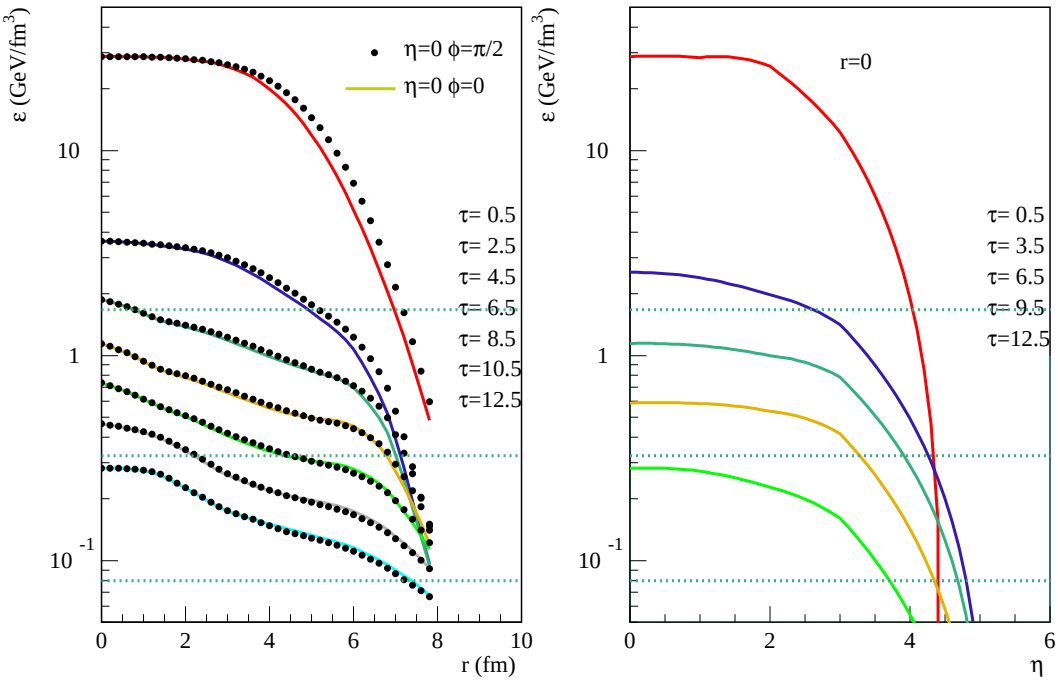

Figure 8: The energy density of the hot dense matter created in the most 10% central Au-Au collisions at 200 AGeV, is plotted as function of the transverse space variable r. Curves from up top to bottom correspond to different proper times, τ=0.5, 2.5, ... (fm/c). The initial time is $\tau_0 = 0.5$fm/c. The solid lines and the corresponding dotted lines refer to $\phi = 0$ and $\phi = \pi/2$, respectively. The two upper horizontal dotted define the mixed phase, the lower horizontal line the freeze-out energy density $\varepsilon_3 = 0.08$ GeV/fm^3.

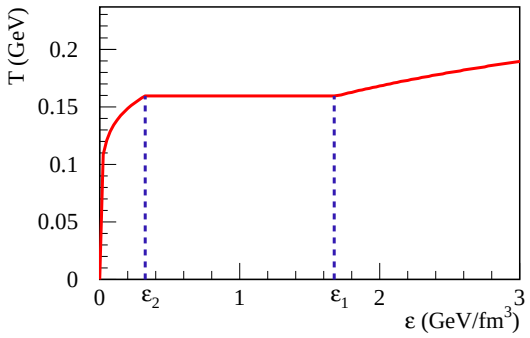

Figure 9: The relation between temperature and energy density. A first-order phase transition happens when $\epsilon(x, y, \eta, \tau) \in (\epsilon_2, \epsilon_1)$ with space-time point (x, y, η, τ) in a mixed phase.

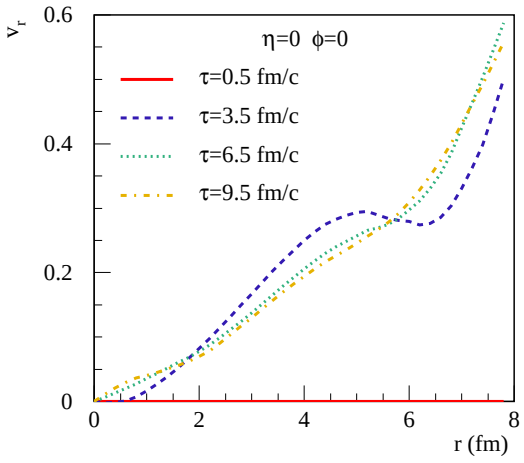

Figure 10: Transverse velocity v_r of the hydrodynamic expansion for the hot dense matter created in the most 10% central Au-Au collisions at 200 AGeV.

with

$$\gamma = \frac{1}{\sqrt{1 - |\vec{v}(\tau, x, y, \eta)|^2}}, \qquad (21)$$

where $\vec{v}(\tau, x, y, \eta)$ is the flow velocity at a given space-time point. The flow rapidity $y = \frac{1}{2}\ln(1 + v_z)/(1 - v_z)$ is roughly equal to the space-time rapidity (as in the Bjorken model). The radial dependence of the transverse velocity v_r is shown in Fig.10, for central Au-Au collisions at 200 AGeV. The large transverse flows at large radii will boost thermal photons to higher $p_{\rm T}$ regions.

In Fig.11 we present the transverse momentum spectra of thermal photons produced in the 10% most central Au-Au collisions at 200 AGeV with an initial time of τ_0=0.5 fm/c. The contributions from the two phases

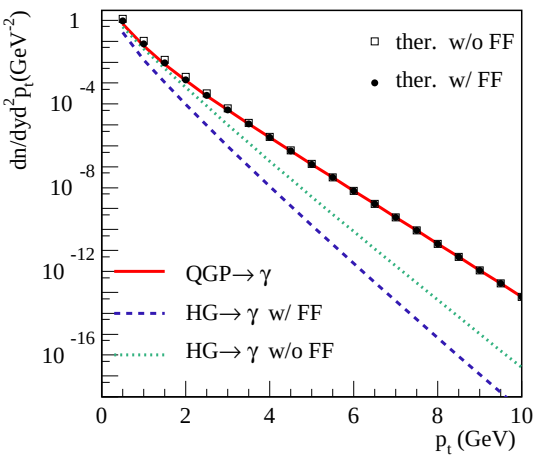

Figure 11: Thermal photons from the most 10% central Au-Au collisions at 200 AGeV with initial time τ_0=0.5 fm/c. The contributions from the two phases are presented separately: QGP phase (solid line) and HG phase (dashed line). The upper limit of the contribution from HG phase, *i.e.*, without consideration of hadron form factor, is presented as dotted line. The total thermal contribution is plotted in the two cases, with hadron form factor (full circles) and without hadron form factor (empty squares).

are presented separately: QGP phase (solid line) and HG phase (dashed line). We can see thermal contribution is dominated by photons from QGP phase, which is much bigger than the upper limit of the contribution from HG phase, *i.e.*, without consideration of hadron form factors (dotted line). The reason is simply that the QGP phase is "hotter" compared to the HG phase. Therefore, hadron form factors makes very little difference concerning the total thermal contribution, as seen in Fig.11, when comparing the complete results with form factor (full circles) and without form factor (empty squares).

IV. HARD PHOTONS FROM PRIMORDIAL N-N SCATTERING, INCLUDING SHADOWING AND ISOSPIN MIXING

Here we present the leading order perturbative calculation of hard photon production, namely the hard photons from primordial N-N scattering. Higher order contributions are related to the production and propagation of jets, so we treat them later. The spectrum of hard photons from a collision between nuclei A and nuclei B is

$$\frac{dN^{AB\to\gamma}}{dyd^2p_{\rm T}} = \sum_{ab}\int dx_a dx_b G_{a/A}(x_a,M^2)G_{b/B}(x_b,M^2) \frac{\hat{s}}{\pi}\frac{d\sigma}{d\hat{t}}(ab\to\gamma+X)\delta(\hat{s}+\hat{t}+\hat{u}) \quad (22)$$

where $G_{a/A}(x_a,M^2)$ and $G_{b/B}(x_b,M^2)$ are parton distribution functions for nuclei A and B. We take MRST 2001 LO parton distributions for protons[18]. Nuclear shadowing effects are taken into account by using EKS98 scale dependent nuclear ratios $R_a^{\rm EKS}(x,A)$[19]. The mixed isospin in nuclei with mass A, neutron number N and proton number Z is taken into account as

$$G_{a/A}(x) = A[\frac{N}{A}G_{a/N}(x)+\frac{Z}{A}G_{a/P}(x)]R_a^{\rm EKS}(x,A). \quad (23)$$

The elementary cross sections after color sum and spin average are given as [17]

$$\frac{d\sigma}{d\hat{t}}(qg\to q\gamma) = -\frac{1}{3}\frac{\pi\alpha\alpha_s}{\hat{s}^2}e_q^2(\frac{\hat{u}}{\hat{s}}+\frac{\hat{s}}{\hat{u}}) \quad (24)$$

$$\frac{d\sigma}{d\hat{t}}(q\bar{q}\to g\gamma) = \frac{8}{9}\frac{\pi\alpha\alpha_s}{\hat{s}^2}e_q^2(\frac{\hat{u}}{\hat{t}}+\frac{\hat{t}}{\hat{u}}), \quad (25)$$

with

$$\alpha_s = \frac{12\pi}{33-2N_f}\frac{1}{\ln(Q^2/\Lambda^2_{\rm QCD})}, \quad (26)$$

and $\Lambda_{\rm QCD}$ = 200 MeV. The 4-momenta of the incoming particles (p_a, p_b) and of the photon (p_γ) in the center-of-mass are

$$p_a = (x_a\frac{\sqrt{s}}{2},\,0,\,0,\,x_a\frac{\sqrt{s}}{2}),\; p_b = (x_b\frac{\sqrt{s}}{2},\,0,\,0,\,-x_b\frac{\sqrt{s}}{2}) \quad (27)$$

and

$$p_\gamma = (p_{\rm T}\cosh y, \vec{p_{\rm T}}, p_{\rm T}\sinh y). \quad (28)$$

The Mandelstam variables are then given as

$$\hat{s} = (p_a+p_b)^2 = x_a x_b s \quad (29)$$

$$\hat{t} = (p_a-p_\gamma)^2 = -x_a\sqrt{s}p_{\rm T}\exp(-y) \quad (30)$$

$$\hat{u} = (p_b-p_\gamma)^2 = -x_b\sqrt{s}p_{\rm T}\exp(y). \quad (31)$$

We set the factorization scale M and renormalization scale Q to be $p_{\rm T}$. Due to the δ-function in Eq.(22), the x_b-integration is trivial, leading to

$$x_b = \frac{x_a x_\perp \exp(-y)}{2x_a - x_\perp\exp(y)}, \quad (32)$$

with $x_\perp = 2p_{\rm T}/\sqrt{s}$. The condition $x_b<1$ requires $x_a\in(x_{\rm min},1)$ with $x_{\rm min} = x_\perp\exp(y)/(2-x_\perp\exp(-y))$. So

$$\frac{dN^{AB\to\gamma}}{dyd^2p_{\rm T}} = \sum_{ab}\int_{x_{\rm min}}^1 dx_a G_{a/A}(x_a,M^2)G_{b/B}(x_b,M^2) \frac{1}{x_a s-\sqrt{s}p_{\rm T}\exp(y)}\frac{\hat{s}}{\pi}\frac{d\sigma}{d\hat{t}}(ab\to\gamma+X). \quad (33)$$

In Fig.12, we plot the corresponding spectrum, for central Au-Au collisions at 200 AGeV. Empty circles present PHENIX data[25]. At high $p_{\rm T}$ region, the contribution of primordial NN collisions is very close the experimental data.

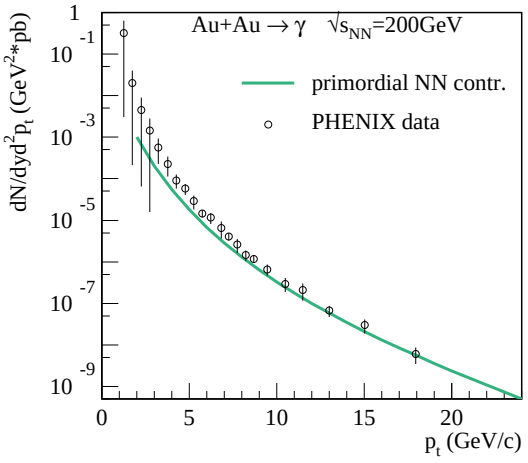

Figure 12: The contribution of primordial NN collisions to direct photon production in the 10% most central Au-Au collisions at 200 AGeV. Isospin mixing and nuclear shadowing are considered. Empty circles present PHENIX data[25].

V. JET PHOTON CONVERSION, INCLUDING JET ENERGY LOSS

When jets propagate in the hot dense matter created in heavy ion collisions, they also interact with the matter and produce direct photons via the Compton process $qg \to q\gamma$ and the quark-antiquark annihilation process $q\bar{q} \to g\gamma$. We denote the momenta of the jet, the thermal parton, and the photon by $p_{\rm jet}$, $p_{\rm th}$ and p, respectively. The leading order QCD Compton and annihilation cross sections are peaked in the forward and backward directions. In the laboratory frame we have $|p_{\rm jet}| \gg |p_{\rm th}| \sim T$, where T is the temperature of the plasma. For high energy photons, i.e. $|p| \gg T$, this implies that $|p| \approx |p_{\rm jet}|$. That is why we call this process a conversion of a jet into a photon with similar momentum. The rate of photon production by annihilation and Compton scattering of jets in the medium can be approximated as [20][21]

$$E\frac{dN}{d^3pd^4x} = \frac{\alpha\alpha_s}{4\pi^2}\sum_q e_q^2 f_q(p,x)T^2\left[\ln\frac{4E_\gamma T}{m_{\rm th}^2} + C\right], \quad (34)$$

with $C = -1.916$, $m_{\rm th}^2 = g^2T^2/6$, and where $\alpha_s = g^2/(4\pi)$ and α are the strong and the electromagnetic couplings. Th subscript "q" denotes all light quark and antiquark species with charge e_q, and $f_q = f_q(\vec{p},x)$ is the phase-space density of partons of flavor q. It is worth emphasizing that the conversion property of the process is reflected in eq.(34) by the fact that the photon spectrum is directly proportional to the parton spectrum f_q. Then at midrapidity the jet-photon conversion contribution to the direct photon production in the most 10% Au-Au collisions is gained via the integration over the space-time evolution of the hot dense matter in QGP phase:

$$\frac{dN^{\rm jet+QGP\to\gamma}}{dyd^2p_{\rm T}} = \int E\frac{dN}{d^3pd^4x}f_{\rm QGP}(x,y,\eta,\tau)dxdyd\eta\tau d\tau. \quad (35)$$

To get f_q, the phase space densities of quarks and antiquarks, we have to fix the geometry of jet formation. The jet production from primordial N-N scattering is assumed to happen at the same proper time $\tau = 0$. Then at $\tau = 0$, the phase space distribution of partons of type q is

$$f_{q_i}(\vec{p},\vec{r},\tau=0) \propto T_A(x-\frac{b}{2},y)T_B(x+\frac{b}{2},y)\delta(z), \quad (36)$$

where b in the impact parameter and T_A and T_B are thickness functions of nuclei A and B. The δ-function is motivated by the strong Lorentz contraction of the colliding nuclei. To have a simple form for a central A-A collision, i.e. most 10% central Au-Au collision, we take the approximation

$$f_q(\vec{p},\vec{r},\tau=0) = \frac{(2\pi)^3}{E}\frac{dN^{AB\to jet(q)}}{dyd^2p_{\rm T}} \frac{2}{\pi R_\perp^2}(1-\frac{r_\perp^2}{R_\perp^2})\theta(R_\perp - r_\perp)\delta(z) \quad (37)$$

where $R_\perp$is the radius of nuclei Au, and with $r_\perp = \sqrt{x^2+y^2}$. The momentum distribution is calculated as

$$\frac{dN^{AB\to\rm jet}}{dyd^2p_{\rm T}} = \sum_{abcd}\int_{x_{\rm min}}^1 dx_a K_{\rm jet}G_{a/A}(x_a,M^2)G_{b/B}(x_b,M^2) \frac{1}{x_as - \sqrt{s}p_{\rm T}\exp(y)}\frac{\hat{s}}{\pi}\frac{d\sigma}{d\hat{t}}(ab\to cd), \quad (38)$$

which is very similar to eq.(33). Here, the cross sections of all possible partonic processes $ab \to cd$ make totally 127 terms[17]. K_{jet}=2 is used to take into account higher order contributions to jet production in our calculation[22]. The phase space distribution of jet satisfies the normalization

$$\int f_q(\vec{p},\vec{r},\tau=0)\frac{d^3rd^3p}{(2\pi)^3} = N_q, \quad (39)$$

where N_q is the number of jets of type q.

If we ignore the jet energy loss due to the interaction between jets and matter, then at any $\tau > 0$, the phase space distribution of jets is

$$f(\vec{p},\vec{r},\tau) = \int d^3r_0 f(\vec{p},\vec{r}_0,\tau=0)\delta(\vec{r}-\vec{r}_0-\vec{v}t) = f(\vec{p},\vec{r}-\vec{v}t,0) \quad (40)$$

where $\vec{v}$ is the velocity of a jet, $\vec{v} = \vec{p}/E$, and $t = \tau cosh(\eta)$ with η being the space time rapidity.

If we consider the modification of the jet energy and its momentum due to the interaction between jets and hot dense matter, then the phase space distribution $f(\vec{p}, \vec{r}, \tau)$ of jets should be replaced by

$$\int d^3r_0 d^3p_0 f(\vec{p_0}, \vec{r}_0, 0)\delta(\vec{p_0} - \frac{\vec{p}}{E}\Delta E - \vec{p})\delta(\vec{r} - \vec{r}_0 - \vec{v}t)$$
$$= \int d^3p_0 f(\vec{p_0}, \vec{r} - \vec{v}t, 0)\delta(\vec{p_0} - \frac{\vec{p}}{E}\Delta E - \vec{p}) \quad (41)$$

with $E = |\vec{p}|$, and where ΔE is the energy loss of a jet propagates from the formation point $(\vec{r}_0, 0)$ to the jet-medium interaction point $(\vec{r}, \tau)$. In static matter, one has [23]

$$\Delta E_c = \frac{L}{\lambda_c}\epsilon_c, \quad (42)$$

with $\epsilon_c = \alpha_s\sqrt{\mu^2 E/\lambda}_c$, and where the mean free path λ_c of the jet in the medium, and $\mu = gT$, are all temperature dependent quantities. The index "c" refers to the jet type (quark or gluon). Due to the space-time evolution of temperature as $T = T(x, y, \eta, \tau)$, we have to replace L in Eq.(42) by the integration $\int_0^t v\, f_{\rm QGP} dt'$ along the jet's trajectory in the QGP plasma. Light-flavour quarks and gluons are massless, with $v = 1$, and so we get

$$\Delta E = \int_0^t \frac{\epsilon_c(T(x, y, \eta, \tau))}{\lambda_c(T(x, y, \eta, \tau))} f_{\rm QGP}(x, y, \eta, \tau) dt'. \quad (43)$$

The mean free path λ_c is given as

$$\lambda_g^{-1} = \sigma_{gq}\rho_q + \sigma_{gg}\rho_g, \quad (44)$$

$$\lambda_q^{-1} = \sigma_{qq}\rho_q + \sigma_{qg}\rho_g, \quad (45)$$

where the cross sections are given as [24] $\sigma_i = C_i\frac{\alpha\pi}{T^2}$, with $C_{qq} = \frac{4}{9}$, $C_{qg} = 1$ and $C_{gg} = \frac{9}{4}$, and where ρ_q and ρ_g are the thermal parton densities.

Fig.13 shows the jet-photon conversion contribution to direct photon production in central Au-Au collisions at 200 AGeV. We show the results with and without energy loss, together with PHENIX data[25]. We can see that considering energy loss can indeed suppress the jet-photon conversion contribution, by about a factor of three. Obviously, higher jet energies are needed to produce a photon with a given energy, in case of jet energy loss in the medium. The effect from different hydrodynamic initial times τ_0 is also considered. However, results with τ_0=0.5 fm/c and 1 fm/c are indistinguishable. Our results also agree well with the earlier work by Turbide[13], although they use one dimensional hydrodynamics.

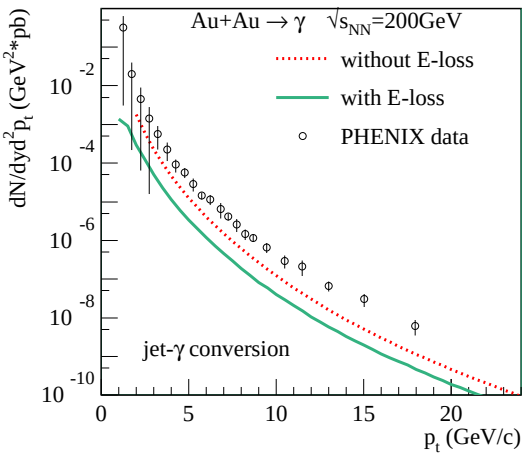

Figure 13: Jet-photon conversion contribution to direct photon production in the 10% most central Au-Au collisions at 200 AGeV. Dotted line: jets traverse the hot dense matter without energy loss; solid line: jets traverse the hot dense matter with energy loss; Empty circles present PHENIX data[25]. The effect from different hydrodynamic initial times τ_0 is also considered. However, results with τ_0=0.5 fm/c and 1 fm/c are indistinguishable.

VI. BREMSSTRAHLUNG PHOTONS, INCLUDING JET ENERGY LOSS

We discussed earlier leading order photon production from elementary NN collisions. However, also higher order diagrams give important contributions. Here, we discuss "bremsstrahlung photons" from jets, also referred to as "jet fragmentation". We can treat the bremsstrahlung contribution via parton fragmentation functions $D_{\gamma/c}(z, Q^2)$ being the probability for obtaining a photon from a jet c, where the photon carries a fraction z of the jet's momentum. The effective fragmentation functions for obtaining photons from partons can be calculated. The leading order result is

$$zD_{\gamma/q}(z, Q^2) = e_q^2\frac{\alpha}{2\pi}[1 + (1 - z)^2]\ln(Q^2/\Lambda^2) \quad (46)$$

and

$$zD_{\gamma/g}(z, Q^2) = 0, \quad (47)$$

where e_q is the fractional charge of the quark q. The photon fragmentation functions evolve with Q^2 just as the usual hadronic fragmentation functions do, as a result of gluon bremsstrahlung and $q\bar{q}$ pair production. The resulting evolution equations are

$$\frac{dD_{\gamma/q_i}(z, Q^2)}{dt} \quad (48)$$
$$= \frac{\alpha_s(Q^2)}{2\pi}\int_z^1 \frac{dy}{y}[D_{\gamma/q_i}(y, Q^2)P_{qq}(z/y)$$
$$+D_{\gamma/g}(z, Q^2)P_{gq}(z/y)],$$

and

$$\frac{dD_{\gamma/g}(z,Q^2)}{dt} = \frac{\alpha_s(Q^2)}{2\pi}\int_z^1 \frac{dy}{y}[\sum_{i=1}^{2N_f} D_{\gamma/q_i}(y,Q^2)P_{qg}(z/y) + D_{\gamma/g}(z,Q^2)P_{gg}(z/y)] \quad (49)$$

where P_{qq}, P_{gq},P_{qg} and P_{qq} are splitting functions appearing in the DGLAP equations. The parameterized solutions from Owens[17] are

$$zD_{\gamma/q_i}(z,Q^2) = \frac{\alpha}{2\pi}[e_i^2\frac{2.21-1.28z-1.29z^2}{1-1.63\ln(1-z)} + 0.002(1-z)^2z^{-1.54}]\ln(Q^2/\Lambda^2), \quad (50)$$

and

$$zD_{\gamma/g}(z,Q^2) = \frac{\alpha}{2\pi}0.0243(1-z)z^{-0.97}\ln(Q^2/\Lambda^2). \quad (51)$$

The bremsstrahlung contribution to direct photon production is then

$$\frac{dN^{jet\to\gamma}}{dyd^2p_T} = \sum_{c=g,q_i}\int dz_c\frac{dN^{AB\to jet_c}}{dyd^2p_T^c}\frac{1}{z_c^2}D_{\gamma/c}(z_c,Q^2), \quad (52)$$

with $p_T^c = p_T/z_c$ being the momentum carried by the jet c before fragmentation, and $d^3p/E = z_c^2d^3p^c/E^c$. The jet cross section can be obtained from Eq.(38).

To take into account the energy loss of the jet in the QGP phase, the bremsstrahlung contribution to direct photon production is modified. We may use a modified fragmentation function[26], given as

$$D_{\gamma/c}(z_c,Q^2,\Delta E_c) = (1-e^{-\frac{L}{\lambda_c}})[\frac{z_c'}{z_c}D^0_{\gamma/c}(z_c',Q^2) + \frac{L}{\lambda_c}\frac{z_g'}{z_c}D^0_{\gamma/g}(z_g',Q^2)] + e^{-\frac{L}{\lambda_c}}D^0_{\gamma/c}(z_c,Q^2), \quad (53)$$

where $z_c' = p_T/(p_T^c - \Delta E_c)$ and $z_g' = (L/\lambda_c)\,p_T/\Delta E_c$ are the rescaled momentum fractions carried by jet c and the emitted gluons before fragmentation, and where $D^0_{\gamma/q}$ and $D^0_{\gamma/g}$ are the original fragmentation functions, given in Eqs.(50) and (51). So a parton c has the probability $\exp(-L/\lambda_c)$ to fragment directly without interacting with the medium, and the probability $1-\exp(-L/\lambda_c)$ to interact with the medium before fragmentation. The ratio L/λ_c represents the number of scatterings, and a gluon of energy ϵ_c is emitted each time when a parton scatters with the medium.

As discussed earlier, the energy loss in the medium with a constant temperature is $\Delta E_c = \frac{L}{\lambda_c}\epsilon_c$, where

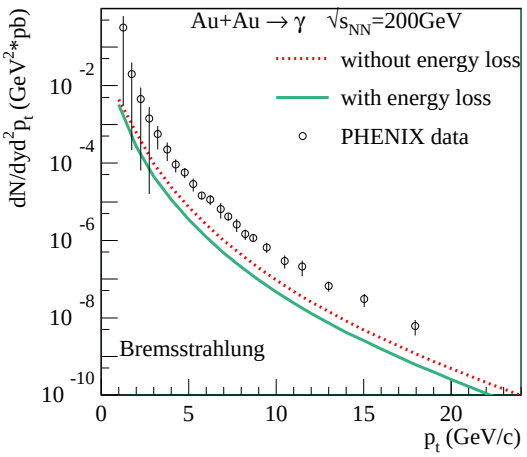

Figure 14: Bremsstrahlungs (= jet fragmentation) contribution to direct photon production in the 10% most central Au-Au collisions at 200 AGeV. Dotted line: jets traverse the hot dense matter directly without energy loss. Solid line: jets traverse the hot dense matter with energy loss. Empty circles: PHENIX data[25].

λ_c is the mean free path of jet c in the medium and $\epsilon_c = \alpha_s\sqrt{\mu^2E/\lambda_c}$. Those quantities are temperature dependent. In our case, the temperature evolves with space and time. So similar to Eq.(43), we replace L/λ_c and ΔE_c by the corresponding mean values, namely

$$\int_{\tau_1}^{\infty}\frac{1}{\lambda_c(T(x,y,\eta,\tau))}f_{QGP}(x,y,\eta,\tau)dt, \quad (54)$$

$$\int_0^{\infty}\frac{\epsilon_c(T(x,y,\eta,\tau))}{\lambda_c(T(x,y,\eta,\tau))}f_{QGP}(x,y,\eta,\tau)dt. \quad (55)$$

We take the mean energy loss per scattering $\lambda\Delta E_c/L$ as the energy carried by each emitted gluon.

In Fig.14, we present the bremsstrahlung contribution to direct photon production, with and without considering energy loss. We can see that the photon production is considerably suppressed due to the energy loss of the jets in the hot dense matter. The results from two different initial times τ_0=0.5 fm/c and 1 fm/c is indistinguishable.

VII. RESULTS AND DISCUSSION

In the following we are going to collect and discuss our results. In Fig.15 we compare the different non-thermal contributions to photon production in central Au-Au collisions at 200 AGeV. We show the contribution from primordial NN collisions (dashed line), bremsstrahlung (or fragmentation) photons (dotted line), and photons from jet-photon conversion (solid line). We have taken into account energy loss of jets in the hot and dense matter, both for bremsstrahlung photons and jet-photon conversion. We also plot PHENIX data[25], as a reference.

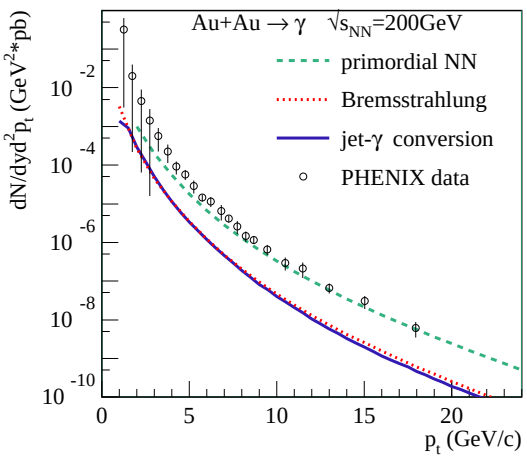

Figure 15: Comparison of the different non-thermal contributions photon production in the 10% most central Au-Au collisions at 200 AGeV. Dashed line: contribution from primordial NN collisions. Dotted line: contribution from Bremsstrahlung. Solid line: jet-photon conversion contribution. Jets energy loss in the hot dense matter is considered both for bremsstrahlung photons and jet-photon conversion. Empty circles: PHENIX data[25].

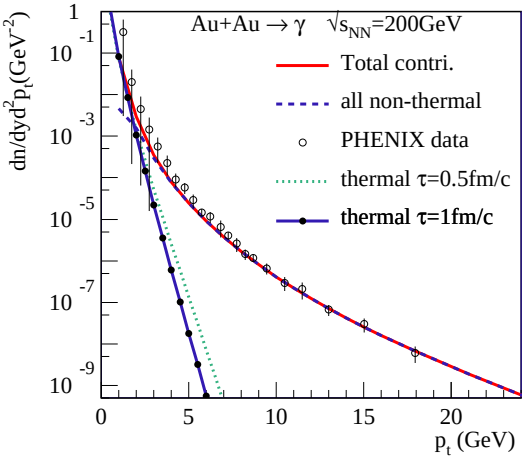

Figure 16: The total contribution (solid line) is compared with PHENIX data[25] (empty circles). Thermal contributions from a hydrodynamic calculation with initial time τ_0=0.5 fm/c is plotted as dotted line, while τ_0=1 fm/c is presented as solid line with full circles. Different values of τ_0 are indistinguishable concerning the total contribution.

Jet-photon conversion contributes the same magnitude as bremsstrahlung, but both are small compared to the hard photons from primordial NN collisions.

In Fig.16, the total contribution (solid line), including all non-thermal and thermal contributions, is compared with PHENIX data[PHENIX data] (empty circles). The thermal contribution from a hydrodynamic calculation with an initial time τ_0=0.5 fm/c is plotted (dotted line) as well as the results of a calculation with τ_0=1 fm/c (solid line with full circles). Smaller τ_0 gives a somewhat broader distribution, but this effect is invisible in the total contribution. At very low $p_{\rm T}$, thermal production dominates the direct photon production. However, the thermal spectra decrease very fast with $p_{\rm T}$, and become negligible for $p_{\rm T}\geq$ 4GeV/c. The hydrodynamic configuration also affects the jet-photon conversion and the bremsstrahlung contribution. But this effect is very weak: taking different initial times within the range [0.5,1]fm/c make very little difference to the total contribution (invisible in Fig.16). The complete contribution, containing all the thermal and non-thermal contributions, follow quite well the PHENIX data.

It is useful to compare the AuAu results with proton-proton, and here it is convenient to study the nuclear modification factor, defined to be ratio of the nuclear spectrum to the proton-proton one, divided by the number $N_{\rm coll}$ of binary collisions. We use $N_{\rm coll}$=880 for the 10% most central Au-Au collisions at 200 AGeV, treated in this paper. We compute the proton-proton differential cross section by using $\sigma^{pp}_{\rm inelastic}$ =40.83mb, and $K_{\rm jet}$=2, and the unmodified photon fragmentation functions given in eq.(50, 51).

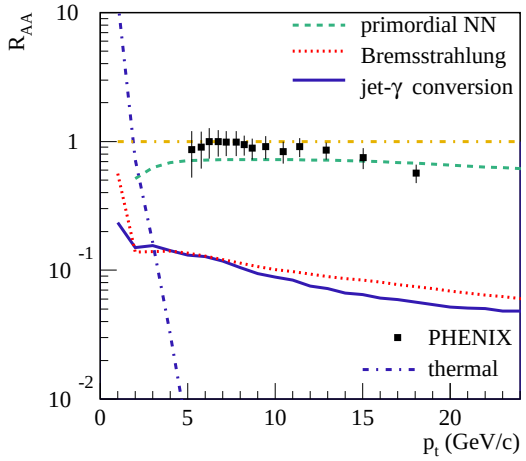

Figure 17: Different non-thermal contributions and thermal contribution to nuclear modification factor R_{AA} is compared with PHENIX data[25] (full squares). Dashed line: the primordial NN contribution; Dotted line: bremsstrahlung; Solid line: jet-gamma conversion; Dotted dashed line: thermal contribution.

In Fig.17, we plot the different non-thermal contributions, namely the primordial NN contribution (dashed line), bremsstrahlung (dotted line), and jet-gamma conversion (solid line). The contributions from bremsstrahlung and jet-photon conversion are of the same magnitude, but one order smaller than that the primordial NN curve. We also show the rapidly falling thermal contribution(dotted dashed line). Above 5 GeV, only photons from primordial NN scattering contribute significantly. This is why we look more closely to this latter contribution.

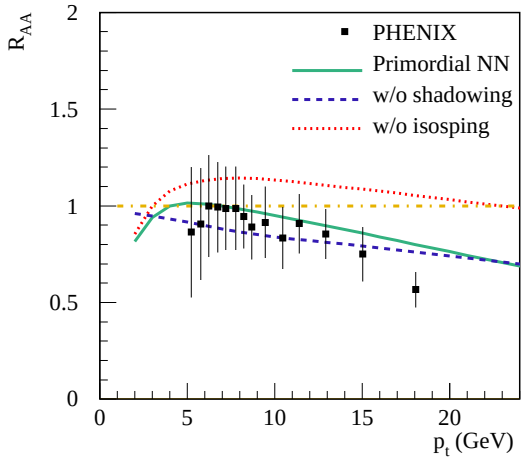

Figure 18: A close look at primordial NN scattering contribute to the nuclear modification factor R_{AA}. Solid line: the complete primordial NN contributions, including isospin mixing and shadowing; Dotted line: omitting isospin mixing (but considering shadowing); Dashed line: omitting shadowing (but considering isospin mixing). Full squares: the same data as in Fig.17.

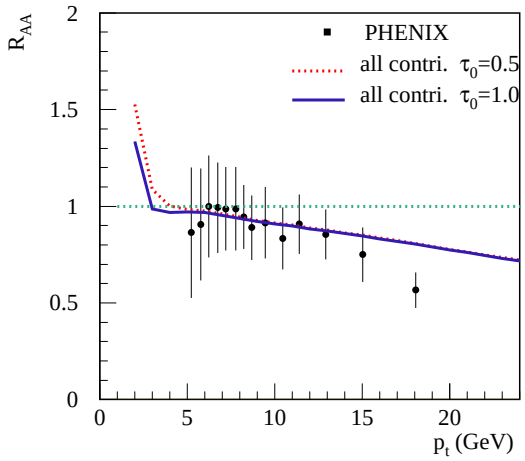

Figure 19: The complete calculation of the nuclear modification factor is compared to PHENIX data[25]. Dotted line: τ_0=0.5 fm/c; solid line: τ_0=1 fm/c. Full squares: the same data as in Fig.17.

In Fig.18, we show again the complete primordial NN contributions, including isospin mixing and shadowing. But we also show the results one would obtain by omitting isospin mixing (but considering shadowing), and by omitting shadowing (but considering isospin mixing). Obviously, both effect are crucial. In particular the isospin mixing is responsible for getting a nuclear modification factor of less than unity.

Finally we show in Fig.19 the complete calculation, for two different options of the initial time for the hydrodynamical evolution. The two curves are almost identical. As mentioned earlier, the total contribution to the nuclear modification factor is less than unity, due to isospin correction. However, the experimental data drop systematically below the theoretical curve, and it seems difficult with the processes discussed in this paper, to get the theoretical curve further down. So maybe some "new physics"? Before answering this question, one should not forget the large uncertainties of the experimental pp reference, which is a fit function passing between strongly fluctuating data points at large pt.

Acknowledgments

This work is supported by the Natural Science Foundation of China under the project No. 10505010 and by MOE of China under project No. IRT0624. F.M.LIU thanks the IN2P3/CNRS and Subatech for their hospitality during her visit in Nantes.

[1] J. Kapusta, P. Lichard and D. Seibert, Phys. Rev. D **44**:2774,(1991);**47**:4171(E),(1991).
[2] P. Aurenche, F. Gelis, R. Kobes and E. Petitgirard, Phys. Rev. D **58**:085003,(1998).
[3] P. Arnold, G. D. Moore and L. G. Yaffe, J. High Energy Phys. **0111**, 057 (2001); J. High Energy Phys. **0112**, 9 (2001).
[4] F. Karsch, Z. Phys. C**38**, 1998,147.
[5] L. Xiong, E. Shuryak and G. E. Brown, Phys. Rev. D **46**:3798,(1992).
[6] C. Song, Phys. Rev. C **47**:2861,(1993).
[7] M.A. Halasz, J.V. Steele, G.Q. Li and G.E. Brown, Phys. Rev. **58**, 365 (1998).
[8] C. Song and G. Fai, Phys. Rev. C **58**:1689,(1998).
[9] S. Turbide, R. Rapp and C. Gale, Phys. Rev. C **69**:014903,(2004).
[10] S. Turbide, R. Rapp and C. Gale, Phys. Rev. C **71**:059803,(2005).
[11] R. Rapp, Mod. Phys. Lett. A **19**, 1717 (2004).
[12] F. Arleo *et al.*, "Photon physics in heavy ion collisions at the LHC," arXiv:hep-ph/0311131, CERN Yellow Report on Hard Probes in Heavy Ion Collisions at the LHC.

[13] S. Turbide, C. Gale, S. Jeon and G. Moore, Phys. Rev. C **72**:014906,2005.
[14] K. Werner, Phys. Rev. Lett. 98, 152301 (2007);
[15] K. Werner, F.M. Liu, T. Pierog, Phys. Rev. C 74, 044902 (2006)
[16] Y. Hama, T. Kodama and O. Socolowski Jr., Braz. J. Phys. **35**, 24 (2005).
[17] J.F. Owens, Rev. Mod. Phys. 59, 465 (1987).
[18] A.D. Martin, R.G. Roberts, W.J. Stirling and R.S. Thorne hep-ph/0201xxx.
[19] K.J. Eskola, V.J. Kolhinen and C.A. Salgado, Eur. Phys. J. C9 (1999) 61; K.J. Eskola, V.J. Kolhinen and P.V. Ruuskanen, Nucl. Phys. **B535** (1998) 351.
[20] C.Y.Wang, Introduction to high-energy heavy ion collisions (World Scientific Singapore, 1994).
[21] R.J. Fries, B.Müller and D.K.Srivastava, Phys. Rev. Lett. **90**, 132301 (2003).
[22] R.J. Fries, B.M\"uller and D.K.Srivastava,Phys. Rev. **C72**, 041902(R), 2005.
[23] R. Baier, Yuri L. Dokshitzer, Alfred H. Mueller, S. Peigne, D. Schiff, Nucl.Phys.**B483**:291-320,1997; Nucl.Phys.**B484**:265-282,1997.
[24] Miklos Gyulassy and Xin-nian Wang, Nucl.Phys.**B420**:583-614,1994.
[25] PHENIX Collaboration, Phys. Rev. Lett. **94**, 232301 (2005); PHENIX Collaboration (Tadaaki Isobe for the collaboration) J.Phys.G**34**:S1015-1018,2007.
[26] X.-N. Wang, Phys. Lett. B 595, 165(2004); 570,299(2004).
[22] K_{jet} can be extracted from the ratio of experimental jet date to leading order calculation. We find $K_{jet} \approx 2$ via pp ($p\bar{p}$) collisions at energy range from 27.4GeV to 630GeV.